

# Preparation and magnetic properties of $(\text{Co}_{0.6}\text{Fe}_{0.3}\text{Ni}_{0.1})_{70-x}(\text{B}_{0.811}\text{Si}_{0.189})_{25+x}\text{Nb}_5$ bulk glassy alloys

Yaqiang Dong<sup>1</sup> · Qikui Man<sup>1</sup> · Chuntao Chang<sup>1</sup> · Baolong Shen<sup>2</sup> · Xin-Min Wang<sup>1</sup> · Run-Wei Li<sup>1</sup>

Received: 24 March 2015 / Accepted: 3 June 2015 / Published online: 13 June 2015  
© Springer Science+Business Media New York 2015

**Abstract** The preparation and soft magnetic properties of  $(\text{Co}_{0.6}\text{Fe}_{0.3}\text{Ni}_{0.1})_{70-x}(\text{B}_{0.811}\text{Si}_{0.189})_{25+x}\text{Nb}_5$  ( $x = 0-4$ ) glassy alloys were investigated. This multicomponent system was found to exhibit a distinct glass transition and a wide supercooled liquid region of over 50 K before crystallization. As a result, the  $(\text{Co}_{0.6}\text{Fe}_{0.3}\text{Ni}_{0.1})_{70-x}(\text{B}_{0.811}\text{Si}_{0.189})_{25+x}\text{Nb}_5$  bulk glassy alloys with diameters up to 5 mm were produced by copper mold casting. In addition to high glass-forming ability, the Co-based glassy alloys also exhibit excellent soft-magnetic properties, i.e., saturation magnetization of 0.54–0.72 T, low coercive field of 0.7–1.4 A/m, and high effective permeability of 18,600–22,400 at 1 kHz under a field of 1 A/m. Furthermore, the giant magneto impedance effects of the  $(\text{Co}_{0.6}\text{Fe}_{0.3}\text{Ni}_{0.1})_{68}(\text{B}_{0.811}\text{Si}_{0.189})_{27}\text{Nb}_5$  glassy ribbon at different driving frequencies were also investigated. The results show that the largest impedance ratio is as high as 138 % at the frequency of 2.5 MHz under an ac current of 0.2 mA, together with high field sensitivity of 12.5 %/Oe.

## 1 Introduction

As electronics becomes more prevalent in our daily lives, most users are aware of only a few component types. An internet search will bring up semiconductors, microprocessors and transistors, but little about the magnetic components that are essential to make those devices function. In fact, soft magnetic materials are one of the most important components for power electronics, electronic compass, electronic current transformers [1–3], and so on. Among the magnetic materials, ferromagnetic bulk glassy alloys (BGAs) are an important components due to their excellent magnetic properties, and since the Fe-(Al, Ga)-metalloid system was synthesized for the first time in 1995 [4], a number of Fe- and Co-based BGAs have been developed for the purpose of applications as functional and structural materials [5–12]. Among them, Co-based BGAs are drawing increasing attention due to their excellent soft-magnetic properties, such as high saturation magnetization ( $I_s$ ), low coercive field ( $H_c$ ) and high effective permeability ( $\mu_e$ ) [8, 10, 13], especially for the amorphous wire and ribbons, which exhibit giant magneto-impedance (GMI) effect, that can be developed as high-sensitivity sensor materials [14–16]. However, due to its poor glass-forming ability (GFA), it was difficult to produce a large amount of high quality fully amorphous wires, which limits the extensive practical applications. So it is important to improve the GFA of Co-based glassy alloys. Recently,  $(\text{Co}_{0.6}\text{Fe}_{0.3}\text{Ni}_{0.1})_{67}\text{B}_{22.7}\text{Si}_{5.3}\text{Nb}_5$  BGA with diameters up to 4.5 mm was synthesized by copper mold casting [17]. In this study, with the aim of further improving the GFA of the Co-based BGAs, as well as developing high-sensitivity sensor materials, we investigated the effect of B and Si contents on thermal stability of the supercooled liquid and cooling behavior of this alloy system. As a result,

✉ Chuntao Chang  
ctchang@nimte.ac.cn

✉ Baolong Shen  
blshen@seu.edu.cn

Yaqiang Dong  
dongyq@nimte.ac.cn

<sup>1</sup> Zhejiang Province Key Laboratory of Magnetic Materials and Application Technology, Key Laboratory of Magnetic Materials and Devices, Ningbo Institute of Materials Technology and Engineering, Chinese Academy of Sciences, Ningbo 315201, China

<sup>2</sup> School of Materials Science and Engineering, Southeast University, No. 2 Southeast University Road, Jiangning District, Nanjing 211189, China

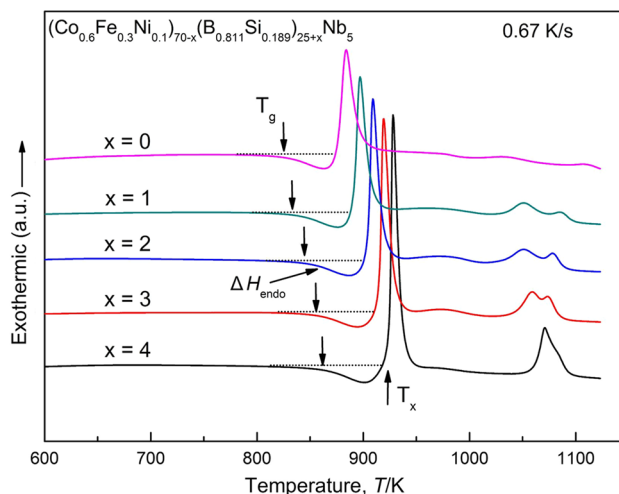
Co-based BGAs  $(\text{Co}_{0.6}\text{Fe}_{0.3}\text{Ni}_{0.1})_{70-x}(\text{B}_{0.811}\text{Si}_{0.189})_{25+x}\text{Nb}_5$  ( $x = 0-4$ ) with diameters up to 5 mm were successfully synthesized by copper mold casting. This paper reports the preparation and magnetic properties of  $I_s$ ,  $H_c$ ,  $\mu_e$  and GMI effect for the  $(\text{Co}_{0.6}\text{Fe}_{0.3}\text{Ni}_{0.1})_{70-x}(\text{B}_{0.811}\text{Si}_{0.189})_{25+x}\text{Nb}_5$  glassy alloys.

## 2 Experimental procedure

Multi-component (Co,Fe,Ni)–B–Si–Nb alloy ingots with nominal compositions of  $(\text{Co}_{0.6}\text{Fe}_{0.3}\text{Ni}_{0.1})_{70-x}(\text{B}_{0.811}\text{Si}_{0.189})_{25+x}\text{Nb}_5$  ( $x = 0-4$ ) were prepared by arc melting the mixtures of pure Co, Fe, Ni and Nb metals, and pure B and Si crystals in an argon atmosphere. Cylindrical alloy rods with different diameters of 1–6 mm were produced by copper mold casting. The structures of the samples were identified by X-ray diffraction (XRD) with  $\text{Cu K}\alpha$  radiation. Thermal stability associated with glass transition temperature ( $T_g$ ), crystallization temperature ( $T_x$ ), and supercooled liquid region ( $\Delta T_x = T_x - T_g$ ) was examined by differential scanning calorimetry (DSC) at a heating rate of 0.67 K/s. The liquidus ( $T_l$ ) temperatures were measured by cooling the molten alloy samples with DSC at a cooling rate of 0.067 K/s. Magnetic properties of  $I_s$ ,  $H_c$  and  $\mu_e$  were measured with a vibrating sample magnetometer under an applied field of 400 kA/m, a  $B$ – $H$  loop tracer under a field of 800 A/m, and an impedance analyzer under a field of 1 A/m, respectively. The impedance measurements were performed by a HP4294A impedance analyzer with four terminal contacts and the test frequency is in the range of 1 kHz–10 MHz. The amplitude of the ac current was kept at constant value of 0.2 mA during the sweep of the applied field.

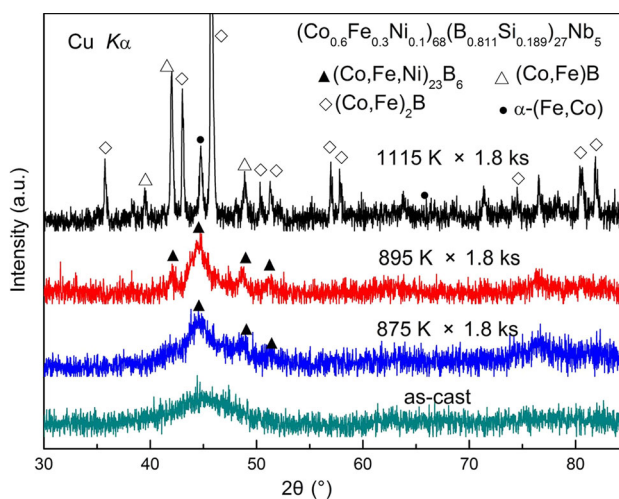
## 3 Results and discussion

Figure 1 shows the DSC curves of the  $(\text{Co}_{0.6}\text{Fe}_{0.3}\text{Ni}_{0.1})_{70-x}(\text{B}_{0.811}\text{Si}_{0.189})_{25+x}\text{Nb}_5$  ( $x = 0-4$ ) glassy alloys produced by melt spinning. It is seen that all of the alloys exhibit distinct glass transition, followed by a large  $\Delta T_x$  of over 50 K, and then crystallization. With increasing the B and Si contents from  $x = 0$  to 4, the  $T_g$  gradually increases from 825 to 862 K, while the  $T_x$  quickly increases from 875 to 925 K, leading to an increase of  $\Delta T_x$  from 50 to 63 K. In addition, for these glassy alloys, it is clearly seen that the area of endothermic peak, that is, the enthalpy of supercooled liquid ( $\Delta H_{\text{endo}}$ ) increases from 19.4 to 26.5 J/g with increasing the B and Si contents. The  $\Delta H_{\text{endo}}$  value indicates the stability of the supercooled liquid, so it is considered that the thermal stability of the supercooled liquid increases with increasing the B and Si contents. The



**Fig. 1** DSC curves of melt-spun  $(\text{Co}_{0.6}\text{Fe}_{0.3}\text{Ni}_{0.1})_{70-x}(\text{B}_{0.811}\text{Si}_{0.189})_{25+x}\text{Nb}_5$  ( $x = 0, 1, 2, 3$  and 4) glassy alloy ribbons

crystallization behaviour of these glassy alloys was investigated by XRD measurement. Figure 2 shows XRD patterns of the  $(\text{Co}_{0.6}\text{Fe}_{0.3}\text{Ni}_{0.1})_{68}(\text{B}_{0.811}\text{Si}_{0.189})_{27}\text{Nb}_5$  glassy alloy subjected to annealing for 1.8 ks at 875 and 895 K, which are between  $T_g$  and  $T_x$ , and for 1.8 ks at 1115 K, corresponding to the temperature just above the second exothermic peaks, respectively. The XRD pattern of the as-spun glassy alloy is also shown for comparison. It can be seen that after the long time annealing of 1.8 ks at 875 and 895 K, some crystalline peaks can be seen. However, a broad halo pattern was still observed clearly, which means that glassy and crystalline phases coexist and has the high thermal stability in the supercooled liquid region. The primary crystalline phase was identified to



**Fig. 2** XRD patterns of the  $(\text{Co}_{0.6}\text{Fe}_{0.3}\text{Ni}_{0.1})_{68}(\text{B}_{0.811}\text{Si}_{0.189})_{27}\text{Nb}_5$  glassy alloy samples annealed for 1.8 ks at 875, 895 and 1115 K, respectively. The pattern of the as-spun glassy alloy is also shown for comparison

(Co,Fe,Ni)<sub>23</sub>B<sub>6</sub> phase, which is consistent with the former results obtained from Co-based BGAs [18]. We also confirmed that the structure after annealing for 1.8 ks at 1115 K consisted of  $\alpha$ -(Fe,Co), (Co,Fe)B and (Co,Fe)<sub>2</sub>B phases. Therefore, it is concluded that the primary precipitation phase of the (Co,Fe,Ni)<sub>23</sub>B<sub>6</sub> is in a metastable state. The primary precipitation of the Fe<sub>23</sub>C<sub>6</sub>-type phase having a complex fcc structure with a large lattice parameter of 1.12 nm including 96 atoms [19], from the network-like structure requires long-range atomic rearrangements of constituent elements, leading to the high stability of the supercooled liquid against crystallization [20]. The cooling behaviours of the (Co<sub>0.6</sub>Fe<sub>0.3</sub>Ni<sub>0.1</sub>)<sub>70-x</sub>(B<sub>0.811</sub>Si<sub>0.189</sub>)<sub>25+x</sub>Nb<sub>5</sub> ( $x = 0-4$ ) glassy alloys were also investigated. As shown in Fig. 3, with increasing B and Si contents from  $x = 0$  to 2, the  $T_1$  decreases from 1453 to 1283 K rapidly, with further increasing B and Si contents to  $x = 4$ , the  $T_1$  increases to 1374 K again, which means that increasing B and Si contents to  $x = 2$  is effective in decreasing  $T_1$  of the alloy system. As a result, the reduced glass transition temperatures ( $T_g/T_1$ ) of these glassy alloys lie in a high value range of 0.568–0.657, and the parameter of  $\gamma [= T_x/(T_g + T_1)]$  also lies in a high value range of 0.384–0.414. Further more, for the alloy with  $x = 2$ , there are only two exothermic peaks and the interval of the two exothermic peaks is quite small (24 K). All these features mean that the alloy composition of  $x = 2$  approaches a deep eutectic point. Besides, the high value of  $T_g/T_1$  reflects a low critical cooling rate for glass formation [21], in this alloy system, the alloy of  $x = 2$  exhibits the highest  $T_g/T_1$  of 0.657, implying this alloy may exhibit high GFA, compared with the other alloys in this alloy system.

Based on the results obtained from the heating and cooling curves of DSC measurements, it is expected that

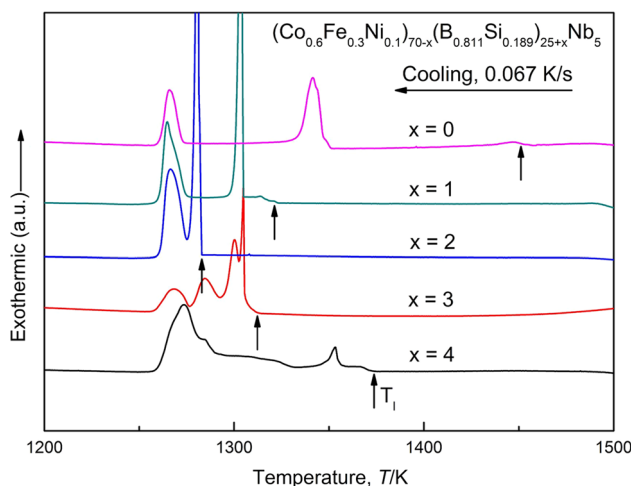


**Fig. 3** DSC curves of (Co<sub>0.6</sub>Fe<sub>0.3</sub>Ni<sub>0.1</sub>)<sub>70-x</sub>(B<sub>0.811</sub>Si<sub>0.189</sub>)<sub>25+x</sub>Nb<sub>5</sub> ( $x = 0, 1, 2, 3$  and 4) alloys

this Co-based glassy alloy system exhibits high GFA. Then, we tried to prepare cylindrical glassy rods with different diameters up to 6 mm by copper mold casting. The glassy alloy rods were produced at all alloy compositions in this system. The critical diameters of glassy alloy rods were 2.5, 4, 5, 4.5 and 3.5 mm for the alloys of  $x = 0, 1, 2, 3,$  and 4, respectively. Figure 4 shows XRD patterns of those cast alloy rods with diameters of 2.5, 4, 5, 4.5 and 3.5 mm, respectively. Only broad peaks without a crystalline peak can be seen for all of these rods, indicating the preparation of a glassy single phase in the diameter range up to 5 mm. The inset in Fig. 4 shows the outer surface and morphology of the cast glassy alloy rods with diameters of 4, 4.5 and 5 mm. Their as-cast surfaces all appear smooth and lustrous. No apparent volume reductions can be recognized on their surfaces, indicating that there was no drastic crystallization during the preparation of these samples. These results indicate clearly the preparation of Co-based glassy alloy rods with diameters up to 5 mm.

Figure 5 shows the changes of  $I_s$ ,  $H_c$  and  $\mu_c$  at 1 kHz as a function of parameter  $x$  for the (Co<sub>0.6</sub>Fe<sub>0.3</sub>Ni<sub>0.1</sub>)<sub>70-x</sub>(B<sub>0.811</sub>Si<sub>0.189</sub>)<sub>25+x</sub>Nb<sub>5</sub> glassy alloys, the samples were annealed for 300 s at temperatures of  $T_g - 50$  K to improve the soft-magnetic properties through structural relaxation. It can be seen that with increasing B and Si contents from  $x = 0-4$ , the  $I_s$  decreases monotonously from 0.72 to 0.54 T, which can be attributed to the decrease of magnetic moment caused by the decreasing of Fe, Co, and Ni contents and hence weakened the chemical short range ordering in the amorphous state. The  $H_c$  is 1.4 A/m for the alloy of  $x = 0$ , followed by a monotonous decrease to 0.7 A/m at  $x = 2$  and then increases to 1.3 A/

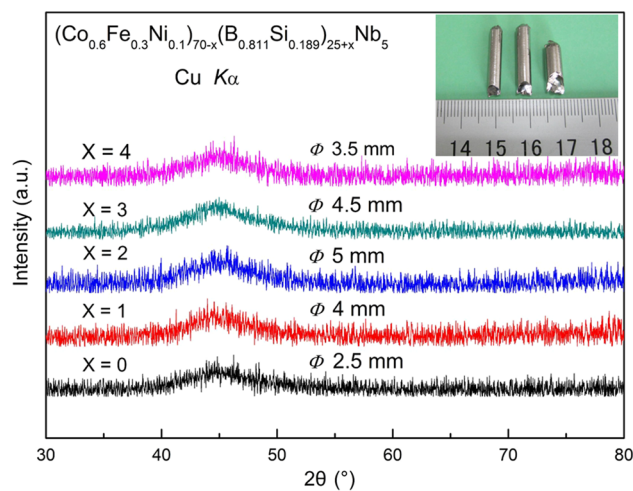


**Fig. 4** XRD patterns of the cast (Co<sub>0.6</sub>Fe<sub>0.3</sub>Ni<sub>0.1</sub>)<sub>70-x</sub>(B<sub>0.811</sub>Si<sub>0.189</sub>)<sub>25+x</sub>Nb<sub>5</sub> ( $x = 0, 1, 2, 3$  and 4) alloy rods with critical diameters of 2.5, 4, 5, 4.5, and 3 mm, respectively. The inset shows the outer surface and morphology of the cast glassy alloy rods with diameters of 4, 4.5 and 5 mm

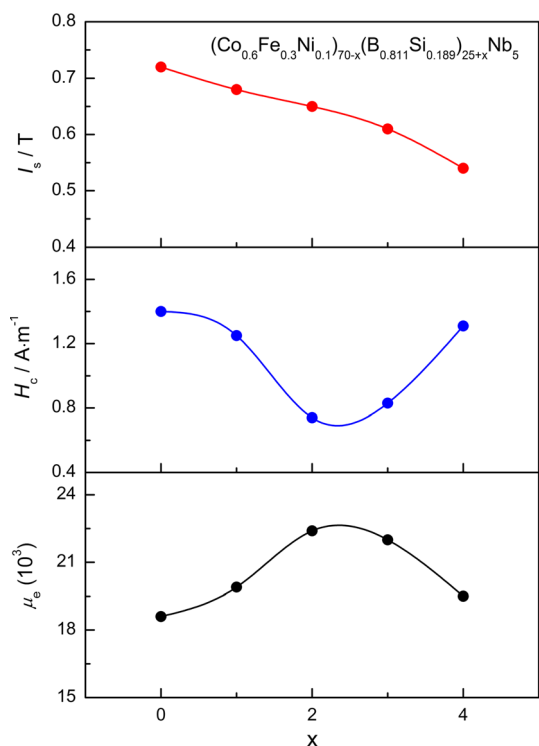


**Fig. 5** Changes in  $I_s$ ,  $H_c$  and  $\mu_e$  at 1 kHz as a function of parameter  $x$  for the  $(\text{Co}_{0.6}\text{Fe}_{0.3}\text{Ni}_{0.1})_{70-x}(\text{B}_{0.811}\text{Si}_{0.189})_{25+x}\text{Nb}_5$  glassy alloy ribbons annealed for 300 s at  $T_g$ -50 K

m, meanwhile, the glassy alloys show high values of  $\mu_e$ , which lies in the range of 18,600–22,400.

Table 1 summarizes the maximum diameter, thermal stability and magnetic properties of the  $(\text{Co}_{0.6}\text{Fe}_{0.3}\text{Ni}_{0.1})_{70-x}(\text{B}_{0.811}\text{Si}_{0.189})_{25+x}\text{Nb}_5$  glassy alloys. In addition to high GFA, this Co-based BGA system also exhibits excellent soft magnetic properties, i.e., high  $I_s$  of 0.54–0.72 T, low  $H_c$  of 0.7–1.4 A/m and high  $\mu_e$  of 18,600–22,400 at 1 kHz under a field of 1 A/m. In particular, the alloy with  $x = 2$  has the highest GFA (5 mm in diameter) and good soft-magnetic properties, i.e., the low  $H_c$  of 0.7 A/m, the high  $I_s$  of 0.65 T and the high  $\mu_e$  of 22,400 at 1 kHz, respectively.

As we know, soft ferromagnetic materials exhibit GMI effect, which is very important for high-performance magnetic sensors [22]. In present Co-based alloy system, as the  $(\text{Co}_{0.6}\text{Fe}_{0.3}\text{Ni}_{0.1})_{68}(\text{B}_{0.811}\text{Si}_{0.189})_{27}\text{Nb}_5$  glassy alloy exhibits excellent soft-magnetic properties, which may show large GMI effect, we also investigated the GMI effect of this alloy using the ribbons. The GMI profiles ( $\Delta Z/Z$ ) were measured as a function of the external dc magnetic field ( $H_{dc}$ ) at various frequencies up to  $f = 10$  MHz. The results are shown in Fig. 6. The effect of two different magnetization dynamics (domain wall motion and rotation) is demonstrated in the GMI curves. It can be seen that at low frequencies ( $f < 1.8$  MHz), the maximum  $\Delta Z/Z$  was observed at near zero field and the GMI profile had a single-peak feature. In this case, the magnetization process is still dominated by the domain wall dynamics. However, as the frequency increased up to 10 MHz, the single peak behavior evolved to a double peak behavior resulting in a deep minimum at zero field and two well pronounced peaks at the anisotropy field,  $H_k$ . Therefore, at 10 MHz, the domain wall motion is strongly damped and the rotational process mainly contributes to the impedance change [23]. In this process, the quasi-free magnetisation responds quickly to the external oscillating magnetic field and gives rise to a large transverse permeability [24]. Consequently, the GMI ratio reached a maximum value and exhibited a two-peak feature in the GMI curve. On the other hand, it is noted that at the frequency of  $f = 2.5$  MHz, the maximum  $\Delta Z/Z$  is as high as 138 %, which is about seven times compares with the value at  $f = 200$  kHz. The higher  $\Delta Z/Z$  value is likely due to the presence of its special domain structure as transverse domains formed by a magnetomechanical coupling between internal stress and magnetostriction [25, 26]. Further increases the frequency, the two-peak feature becomes more clearly and the maximum  $\Delta Z/Z$  decreases gradually, however, it still maintains 80 % at the frequency of 10 MHz.

The frequency dependence of the maximum GMI ratio [ $(\Delta Z/Z)_{\max}$ ] is shown in Fig. 7. In the frequency range of 0.1–10 MHz, the GMI effect first increases with increasing

**Table 1** Maximum diameter, thermal stability, and magnetic properties of cast  $(\text{Co}_{0.6}\text{Fe}_{0.3}\text{Ni}_{0.1})_{70-x}(\text{B}_{0.811}\text{Si}_{0.189})_{25+x}\text{Nb}_5$  ( $x = 0, 1, 2, 3, 4$ ) glassy alloy rods

Alloy	$D_{\max}$ (mm)	Thermal stability						Magnetic properties		
		$T_g$ (K)	$\Delta T_x$ (K)	$T_l$ (K)	$T_g/T_l$	$\gamma$	$\Delta H_{\text{endo}}$ (J/g)	$I_s$ (T)	$H_c$ ( $\text{Am}^{-1}$ )	$\mu_e$
$x = 0$	2.5	825	50	1453	0.568	0.384	19.4	0.72	1.4	18,600
$x = 1$	4	835	55	1322	0.632	0.413	22.1	0.68	1.2	19,900
$x = 2$	5	844	60	1283	0.657	0.425	24.4	0.65	0.7	22,400
$x = 3$	4.5	853	62	1314	0.649	0.422	25.7	0.61	0.8	22,000
$x = 4$	3.5	862	63	1374	0.627	0.414	26.5	0.54	1.3	19,500

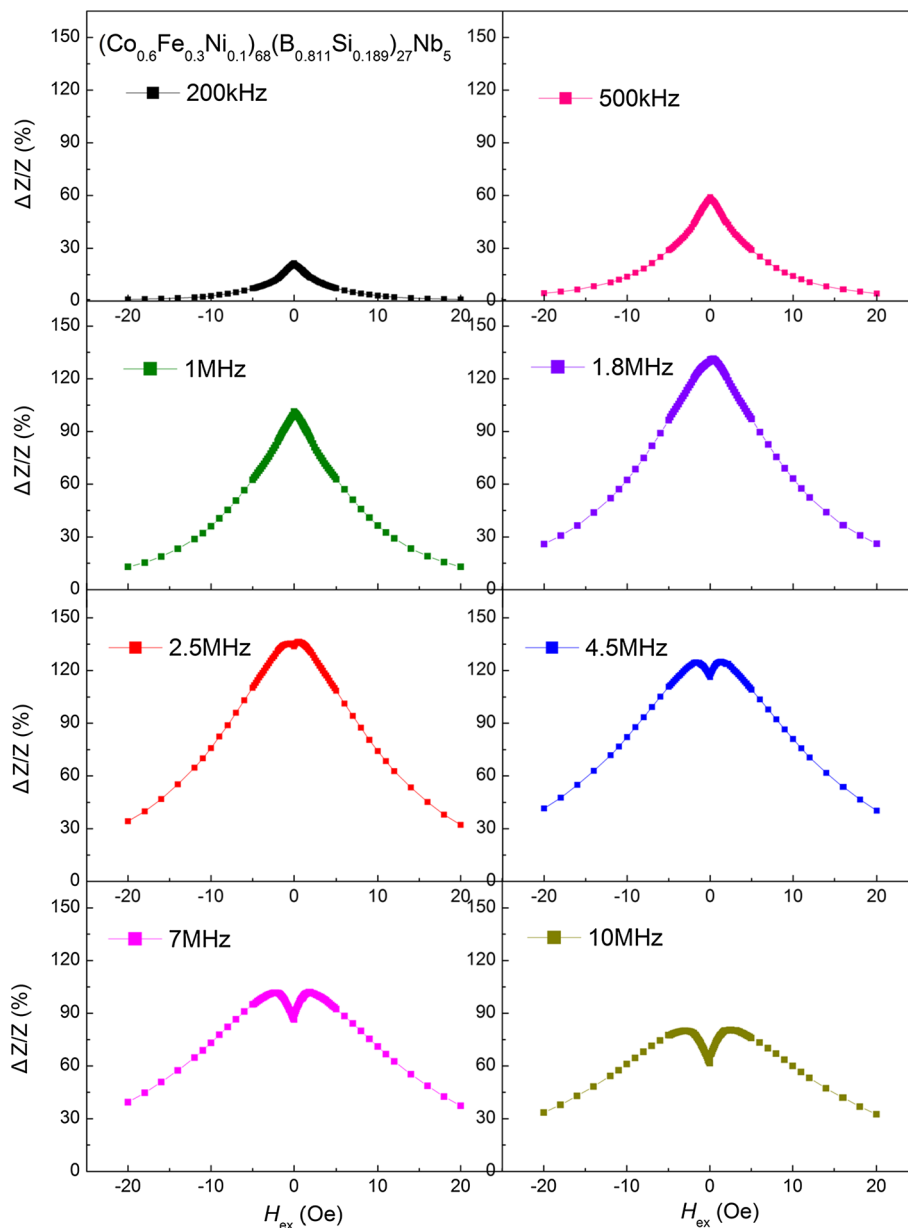


**Fig. 6** GMI profile measured as a function of the external magnetic field at different frequencies for the  $(\text{Co}_{0.6}\text{Fe}_{0.3}\text{Ni}_{0.1})_{68}(\text{B}_{0.811}\text{Si}_{0.189})_{27}\text{Nb}_5$  glassy alloy ribbon

frequency up to 2.5 MHz and then decreases at higher frequencies. This trend can be interpreted by considering the relative contributions of domain wall motion and magnetization rotation to the transverse permeability and hence the GMI effect [27, 28]. The frequency dependence of the field sensitivity of GMI ( $\xi$ ) also shows the similar behaviour. As shown in Fig. 8, the  $\xi$  first increases drastically at low frequencies and reaches to the maximum value of 15 %/Oe at  $f = 1$  MHz, which is more than two times compared with the value at  $f = 200$  kHz. Further

increasing the frequency, the  $\xi$  decreases smoothly to 4.9 % at  $f = 10$  MHz.

Table 2 summarizes the maximum GMI ratio and field sensitivity of the  $(\text{Co}_{0.6}\text{Fe}_{0.3}\text{Ni}_{0.1})_{68}(\text{B}_{0.811}\text{Si}_{0.189})_{27}\text{Nb}_5$  glassy alloy ribbon compared with different alloy systems reported previously [25, 28–31]. The glassy alloy ribbon exhibits rather high maximum GMI ratio of 138 % which is higher than those of the previously reported alloy systems, together with high field sensitivity of 12.5 %/Oe. It is therefore concluded that the  $(\text{Co}_{0.6}\text{Fe}_{0.3}\text{Ni}_{0.1})_{68}(\text{B}_{0.811}\text{Si}_{0.189})_{27}\text{Nb}_5$

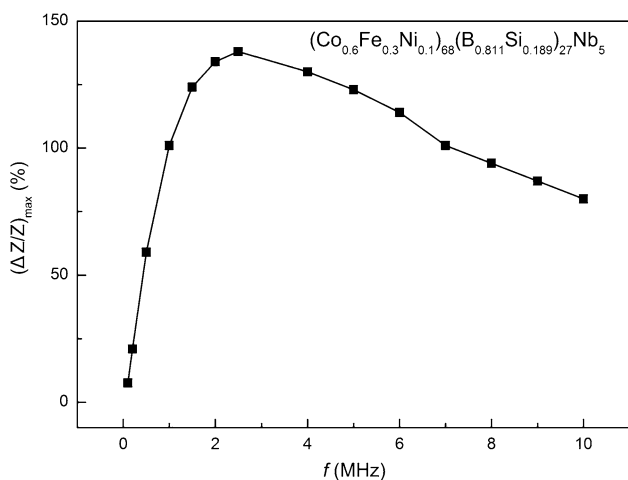


**Fig. 7** The frequency dependence of the maximum GMI ratio  $[(\Delta Z/Z)_{\max}]$  for the  $(\text{Co}_{0.6}\text{Fe}_{0.3}\text{Ni}_{0.1})_{68}(\text{B}_{0.811}\text{Si}_{0.189})_{27}\text{Nb}_5$  glassy alloy ribbon

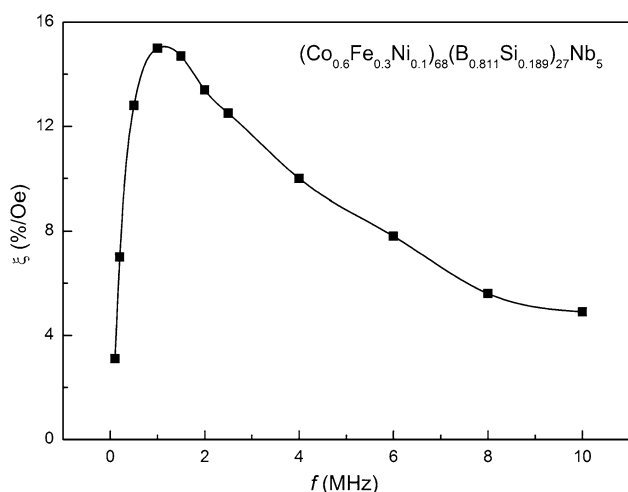


**Fig. 8** The frequency dependence of the field sensitivity of GMI ( $\xi$ ) for the  $(\text{Co}_{0.6}\text{Fe}_{0.3}\text{Ni}_{0.1})_{68}(\text{B}_{0.811}\text{Si}_{0.189})_{27}\text{Nb}_5$  glassy alloy ribbon

glassy alloy ribbon is attractive candidates for making highly sensitive magnetic sensors.

Finally, we discuss why  $(\text{Co}_{0.6}\text{Fe}_{0.3}\text{Ni}_{0.1})_{70-x}(\text{B}_{0.811}\text{Si}_{0.189})_{25+x}\text{Nb}_5$  glassy alloys exhibit a high GFA and good soft-magnetic properties. First, the essential structural feature in  $(\text{Co}_{0.6}\text{Fe}_{0.3}\text{Ni}_{0.1})_{70-x}(\text{B}_{0.811}\text{Si}_{0.189})_{25+x}\text{Nb}_5$  ferromagnetic BGA system is the distorted dense random network of trigonal prisms connected with each other through glue atoms of Nb, leading to the high stability of supercooled liquid against crystallization. Second, compared with the  $[(\text{Co}_{1-x}\text{Fe}_x)_{0.75}\text{B}_{0.2}\text{Si}_{0.05}]_{96}\text{Nb}_4$  alloy system [7], the contents of Nb and B, Si elements were increased in present  $(\text{Co}_{0.6}\text{Fe}_{0.3}\text{Ni}_{0.1})_{70-x}(\text{B}_{0.811}\text{Si}_{0.189})_{25+x}\text{Nb}_5$  glassy alloy system, the mixing enthalpies for Nb and Fe, or Co atomic pairs are  $-16$  and  $-25$  kJ/mol, while for Nb and B or Si atomic pairs, the mixing enthalpies are as large as  $-39$  kJ/mol, respectively [32]. The large mixing enthalpies of the atomic pairs lead to the increase of the thermal stability of the supercooled liquid. On the other hand, as shown in Fig. 3, adjusting the B and Si contents to  $x = 2$  can effectively causes the alloy composition to approach the eutectic point, leading to the increases of  $T_g/T_1$  from 0.568 to 0.657, while the parameter of  $\gamma$  increases from 0.384 to 0.425. It can be also seen in Fig. 3 that the temperature interval between exothermic peaks decreases with B and Si contents increasing from  $x = 0-2$ , implying that the alloy composition of  $x = 2$  is close to that of eutectic alloy. These synergistic effects enable us to prepare BGA rods with large diameters up to 5 mm. Further increases B and Si contents to  $x = 4$ , the GFA decreases to 3.5 mm, which may be attributed to the composition of the alloy deviated from the eutectic point as shown in Fig. 3, where the temperature interval increases again when the B and Si contents increase from  $x = 2-4$ . The origin of the low  $H_c$  can be attributed to the low number density of the domain-wall pinning sites [33], resulting from the high

**Table 2** Comparison of different alloy systems for maximum GMI ratio and field sensitivity

Composition	Alloy status	Max dc magnetizing field (Oe)	Frequency (MHz)	Max GMI Ratio (%)	Sensitivity (%/Oe)
$\text{Co}_{69}\text{Fe}_{4.5}\text{Ni}_{1.5}\text{B}_{15}\text{Si}_{10}$ [28]	Amorphous ribbon	120	6	70	7
$\text{Co}_{66}\text{Fe}_4\text{Ni}_1\text{B}_{14}\text{Si}_{15}$ [25]	Amorphous ribbon	150	4	42	–
$\text{Co}_{84.55}\text{Fe}_{4.55}\text{Zr}_7\text{B}_4$ [29]	Surface coated with Co (ribbon)	120	2	24	0.7
$\text{Fe}_{73}\text{Si}_{14}\text{B}_{8.5}\text{Cu}_1\text{Nb}_{3.5}$ [30]	Nanocrystalline ribbon	35	1	58	8
$\text{Co}_{38}\text{Fe}_{38}\text{Cr}_2\text{Si}_8\text{B}_{14}$ [31]	Amorphous wire	95	0.4	121	96
$(\text{Co}_{0.6}\text{Fe}_{0.3}\text{Ni}_{0.1})_{68}(\text{B}_{0.811}\text{Si}_{0.189})_{27}\text{Nb}_5$	Amorphous ribbon	60	2.5	138	12.5

degree of amorphicity and structural homogeneity proceeding from the high GFA [4].

## 4 Conclusions

In the present study, the GFA and magnetic properties for the  $(\text{Co}_{0.6}\text{Fe}_{0.3}\text{Ni}_{0.1})_{70-x}(\text{B}_{0.811}\text{Si}_{0.189})_{25+x}\text{Nb}_5$  glassy alloys were investigated. The results obtained are summarized as follows:

1. Co-based BGA system  $(\text{Co}_{0.6}\text{Fe}_{0.3}\text{Ni}_{0.1})_{70-x}(\text{B}_{0.811}\text{Si}_{0.189})_{25+x}\text{Nb}_5$  with high GFA that can be cast into BGA rods with diameters up to 5 mm was successfully synthesized, which exhibits good soft-magnetic properties, i.e., high saturation magnetization of 0.54–0.72 T, low coercive field of 0.7–1.4 A/m, and high effective permeability of 18,600–22,400 at 1 kHz under a field of 1 A/m.
2. The GMI effect of the  $(\text{Co}_{0.6}\text{Fe}_{0.3}\text{Ni}_{0.1})_{68}(\text{B}_{0.811}\text{Si}_{0.189})_{27}\text{Nb}_5$  ribbon at different driving frequencies was also analyzed. The largest impedance ratio ( $\Delta Z/Z$ ) is as high as 138 % at the frequency of 2.5 MHz, together with high field sensitivity of 12.5 %/Oe. These excellent properties lead us to expect that this Co-based ferromagnetic BGA system is promising for future applications as functional materials.

**Acknowledgments** This work was supported by the National Natural Science Foundation of China (Grant Nos. 51271194 and 51301189), Ningbo Science and Technology Innovation Team (Grant No. 2011B82004).

## References

1. A. Goldman, *Magnetic Components for Power Electronics*, (Springer Science, New York, 2002), p.55. doi: [10.1007/978-1-4615-0871-7](https://doi.org/10.1007/978-1-4615-0871-7)
2. P. Ripka, *Sens. Actuator A* **41–42**, 394 (1994)
3. C.T. Liang, K.L. Chen, Y.P. Tsai, N. Chen, *IEEE. T. Power. Deliver.* **30**, 184 (2015)
4. A. Inoue, Y. Shinohara, J.S. Gook, *Mater. Trans., JIM* **36**, 1427 (1995)
5. B.L. Shen, H. Koshiba, H. Kimura, A. Inoue, *Mater. Trans., JIM* **41**, 1478 (2000)
6. B.L. Shen, H. Koshiba, A. Inoue, H. Kimura, T. Mizushima, *Mater. Trans.* **42**, 2136 (2001)
7. W.H. Wang, M.X. Pan, D.Q. Zhao, Y. Hu, H.Y. Bai, *J. Phys.: Condens. Matter* **16**, 3719 (2004)
8. C.T. Chang, B.L. Shen, A. Inoue, *Appl. Phys. Lett.* **88**, 011901 (2006)
9. A. Makino, T. Kubota, M. Makabe, C.T. Chang, A. Inoue, *Mater. Sci. Eng., B* **148**, 166 (2008)
10. Q.K. Man, H.J. Sun, Y.Q. Dong, B.L. Shen, H. Kimura, A. Makino, A. Inoue, *Intermetallics* **18**, 1876 (2010)
11. J.F. Wang, R. Li, N.B. Hua, L. Huang, T. Zhang, *Scr. Mater.* **65**, 536 (2011)
12. A. Inoue, K. Hashimoto (Eds.), *Amorphous and Nanocrystalline Materials*. (Springer, New York, 2001), p.4. doi: [10.1007/978-3-662-04426-1](https://doi.org/10.1007/978-3-662-04426-1)
13. K. Amiya, A. Urata, N. Nishiyama, A. Inoue, *J. Appl. Phys.* **101**, 09N112 (2007)
14. L.V. Panina, K. Mohri, T. Uchiyama, M. Noda, *IEEE Trans. Magn.* **31**, 1249 (1995)
15. D.G. Park, C.G. Kim, J.H. Lee, W.W. Kim, J.H. Hong, *J. Appl. Phys.* **101**, 09N109 (2007)
16. H.Q. Guo, H. Kronmuller, T. Dragon, Z.H. Cheng, B.G. Shen, *J. Appl. Phys.* **89**, 514 (2001)
17. Y.Q. Dong, Q.K. Man, H.J. Sun, B.L. Shen, S.J. Pang, T. Zhang, A. Makino, A. Inoue, *J. Alloys Compd.* **509S**, S206 (2011)
18. B.L. Shen, C.T. Chang, T. Kubota, A. Inoue, *J. Appl. Phys.* **100**, 013515 (2006)
19. M. Imafuku, S. Sato, H. Kosiba, E. Matubara, A. Inoue, *Mater. Trans., JIM* **41**, 1526 (2000)
20. M. Imafuku, C.F. Li, M. Matsushita, A. Inoue, *Jpn. J. Appl. Phys. Part 1* **41**, 219 (2002)
21. Z.P. Lu, Y. Li, S.C. Ng, *J. Non-Cryst. Solids* **270**, 103 (2000)
22. G. Yu, X. Bu, B. Yang, Y. Li, C. Xiang, *IEEE Sens. J.* **11**, 2273 (2011)
23. S. Dwevedia, G. Sreenivasulub, G. Markandeyulu, *J. Magn. Mater.* **322**, 311 (2010)
24. D.X. Chen, J.L. Muñoz, A. Hernando, M. Vázquez, *Phys. Rev. B.* **57**, 10699 (1998)
25. Y.K. Kim, W.S. Cho, T.K. Kim, C.O. Kim, H.B. Lee, *J. Appl. Phys.* **83**, 6575 (1998)
26. H. Lee, K.J. Lee, Y.K. Kim, T.K. Kim, C.O. Kim, S.C. Yu, *J. Appl. Phys.* **87**, 5269 (2000)
27. M.H. Phan, H.X. Peng, *Prog. Mater. Sci.* **53**, 323 (2008)
28. A. Chaturvedi, T. Dhakal, S. Witanachchi, A.T. Le, M.H. Phan, H. Srikanth, *Phys. B* **405**, 2836 (2010)
29. N. Laurita, A. Chaturvedi, C. Bauer, P. Jayathilaka, A. Leary, C. Miller, M.H. Phan, M.E. McHenry, H. Srikanth, *J. Appl. Phys.* **109**, 07C706 (2011)
30. M.H. Phan, H.X. Peng, M.R. Wisnom, S.C. Yu, *J. Appl. Phys.* **98**, 014316 (2005)
31. P. Sarkar, A.B. Mallick, P.K. Roy, A.K. Panda, A. Mitra, *J. Magn. Mater.* **324**, 1551 (2012)
32. F.R. de Boer, R. Boom, W.C.M. Mattens, A.R. Miedema, A.K. Niessen, *Cohesion in Metals* (North-Holland, Amsterdam, 1988), p. 276
33. T. Bitoh, A. Makino, A. Inoue, *J. Appl. Phys.* **99**, 08F102 (2006)